Development of Three-Dimensional Acetone LIF Using a Pulse Burst Laser System

Kyle P. Lynch[1]
Advanced Laser Diagnostics Laboratory, Auburn, AL,36849

Preliminary development of a high-speed three-dimensional laser induced fluorescence system using an acetone tracer is explored. The technique is based on the high-speed scanning and imaging of a ultraviolet laser sheet produced by a home-built Nd:YAG pulse burst laser capable of operating in excess of 1 MHz. The focus of this study is on characterization of a substantial upgrade to the pulse burst laser and the addition of a fourth-harmonic generator to yield 266 nm ultraviolet light capable of efficient acetone excitation. Using this system, high-speed 2-D acetone PLIF is demonstrated at 250 kHz. To transition this planar technique to a scanned volumetric measurement, a detailed analysis of 3-D image reconstruction methods and corrections is conducted using traditional Mie scattering flow visualization of a low-speed axisymmetric jet. Multiple sample visualizations (220 x 220 x 68 voxel resolution) of the jet are presented with the camera and laser operating at 500 kHz. In this configuration, each 3-D image took 136 µsec to acquire. This study of 3-D reconstruction methods is a first step towards accurate 3-D LIF. The presented visualizations demonstrate the ability of volumetric measurement techniques to visualize complex, three-dimensional flow fields, such as turbulent mixing layers.

I. Introduction

Techniques for non-invasive flow diagnostics using lasers have seen drastic improvements in speed and resolution in recent years, due to advances in CCD camera design and the demonstration of high-energy, high-repetition rate laser sources, both capable of operating in the MHz range. These advanced technologies have allowed improved, time-resolved studies of many dynamic flow problems occurring at high speeds with particle scattering flow visualization, particle image velocimetry (PIV), planar laser-induced fluorescence (PLIF), and other methods. Additionally, the magnitude of these advances has made possible entirely new flow diagnostic techniques.

The focus of this work is on the preliminary development of a high-speed three-dimensional laser-induced fluorescence (LIF) system. LIF is based on the absorption and fluorescence of laser light by molecules either already present or introduced into a flow field. The chemical characteristics of particular molecules generate unique absorption spectra, typically in the ultraviolet (UV). Using an appropriate light source with strong spectral overlap, light can be efficiently absorbed by the molecule, raising its energy level. To return to an equilibrium state, both short-term (fluorescence), and long-term (phosphorescence) radiative processes occur, emitting photons within separate, higher-wavelength emission spectra. Acetone has been chosen for this study due to its low cost, safe handling characteristics, and broadband absorption spectrum peaking from 260 to 290 nm which can be strongly excited using the fourth-harmonic output of Nd:YAG lasers at 266 nm. The fluorescence emission is also broadband and peaks from 445 to 480 nm, a range of wavelengths easily detected by CCD sensors. The photophysics and physical qualities of acetone have been well characterized by Lozano et al.[1]; in particular, the independence of the fluorescence signal on pressure and temperature and the quenching of the long-term phosphorescence signal by atmospheric oxygen were reported. These findings have established acetone as a suitable molecular tracer for accurate high-speed fluorescence measurements in fluids, and the technique has been successfully applied for both subsonic and supersonic flow studies.[2,3]

This work expands on the PLIF technique to develop a 3-D LIF system. A number of efforts have been made over the years to develop 3-D flow measurement systems, predominantly using the laser sheet scanning technique.[4-8] In this technique, shown schematically in Figure 1, a laser beam is formed into a sheet using cylindrical lenses and is scanned through the flow field using an optical deflector, such as a rotating mirror. As the laser sheet passes through the flow field, a sequence of images at different planes throughout the flow field is acquired. A 3-D image can then

[1] Undergraduate Research Assistant, Aerospace Engineering Department, 211 Davis Hall, AIAA Student Member.

be reconstructed from the stack of images. The primary advantages of this method are the modest optical access requirements in comparison to holographic and tomographic 3-D imaging, and the compatibility with multiple well-established planar diagnostic techniques.

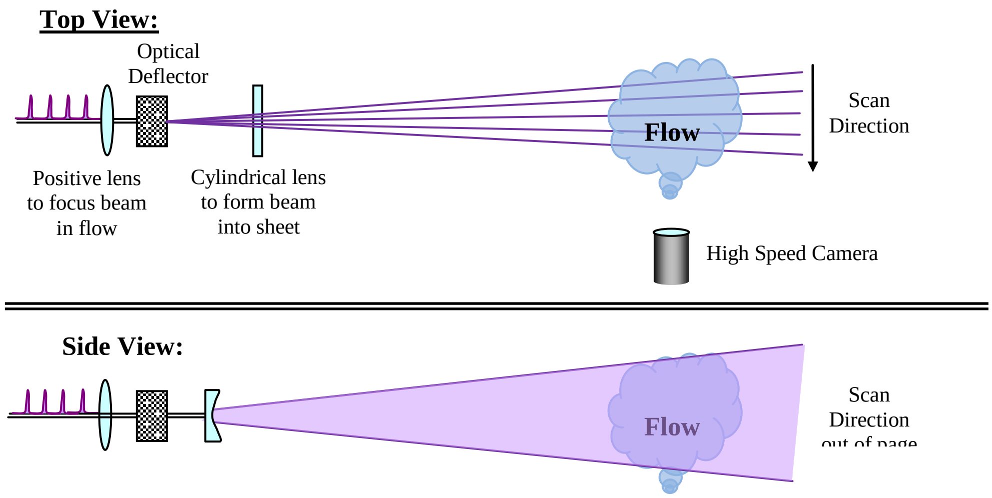

Figure 1. Schematic of 3-D Laser Sheet Scanning LIF Concept, with Ultraviolet Laser Light Fluorescing an Acetone-Seeded Flow Field.

Various factors such as the duration of the laser scan, imaging frame rates, and number of image frames posed inherent limitations in the speed of flows studied and the detail of the reconstructions created in earlier works. To address many of these concerns, a 3-D flow visualization system was developed and demonstrated by Thurow and Lynch[9], utilizing a MHz-rate pulse burst laser, galvanometric scanning mirror, and ultra high-speed camera. This system was employed to conduct a study of modal structure in a turbulent jet using the 2nd-harmonic light output from the pulse burst laser for Mie scattering flow visualization.[10] A significant limitation encountered in this study was the limited fundamental laser pulse energy available from the system at the time (~1 mJ/pulse), restricting the dynamic range and increasing the effect of noise in the resulting images. The low energy available at the 2nd-harmonic prevented any further harmonic generation, rendering the system unable to create 4th-harmonic light at 266 nm needed for acetone LIF.

This work achieves two complementary goals that greatly extend the diagnostic capabilities of the 3-D flow visualization system and represent the initial stages in the development of 3-D acetone LIF: completion of a substantial upgrade in energy to the pulse burst laser and the addition of a fourth-harmonic generator. In addition, novel image correction and processing techniques unique to the laser sheet scanning method are described and implemented. These efforts are demonstrated, respectively, by acquiring 2-D acetone PLIF data at 250 kHz on a high-speed flow field, and applying image processing procedures on a low-speed axisymmetric jet seeded with water particles.

II. Pulse Burst Laser Upgrade

The pulse burst laser used in the 3-D LIF system is a 3rd-generation design based on an initial design by Wu et al.[11], a 2nd-generation design by Thurow et al.[12], and similar 2nd-generation systems in place elsewhere.[13,14] A thorough description of the design features and performance has been reported previously,[15] however an overview of the system, with emphasis on upgraded components, is provided here.

A. Upgraded Pulse Burst Laser System Design

The configuration of the system is classified a master oscillator power amplifier (MOPA), where a burst of low energy pulses is formed and amplified through a chain of power amplifiers. The master oscillator of the system is a low power (100 mW) continuous-wave Nd:YAG laser operating at 1064 nm, which is “sliced” into a configurable burst of pulses using an Acousto-Optic Modulator (AOM). This device is capable of creating an arbitrary number of pulses, as short as 10 nsec each, with a maximum repetition rate of over 40 MHz. The output beam is propagated approximately 5 feet and through a faraday isolator as an aperture. This additional path length before the aperture acts as a filter to prevent microscopic impurities in the AOM crystal from forward-scattering light into the amplifier chain between pulses. This approach has yielded a contrast ratio of over 15,000:1, previously only attainable by use of a sensitive spatial filter. This contrast is critical to prevent gain drainage from amplification of low intensity light between pulses.

The resulting short, low energy pulses (1 nJ/pulse) enter a series of five flashlamp-pumped Nd:YAG rod amplifiers, with rod diameters of 4, 5, 6.3, 9.5, and 12.7 mm, respectively. The first three amplifiers operate in a double-pass configuration for maximum gain while in the small to moderate signal regime. The two new amplifiers, four and five, are single-passed to minimize gain depletion throughout the duration of the pulse burst. Faraday isolators are placed between each amplifier stage to reduce gain depletion through parasitic oscillations in the system. Figure 2 is a photo of the master oscillator and power amplifier chain. Energy is delivered to the flashlamps using five Analog Modules 8800V pulsed flashlamp controllers in a similar setup to Jiang et al.[16] Starting at the first amplifier and proceeding through the system, each amplifier is increased in energy up to the threshold of parasitic lasing, and delayed to create bursts of pulses with approximately uniform energy. This occurs when the pulses are timed to coincide with the approximately 250 µsec rise time of the flashlamp pump sources. Therefore, the pumping and depletion of excited Nd^{3+} ions in the rods by flashlamp radiation and stimulated emission is kept at a constant level.

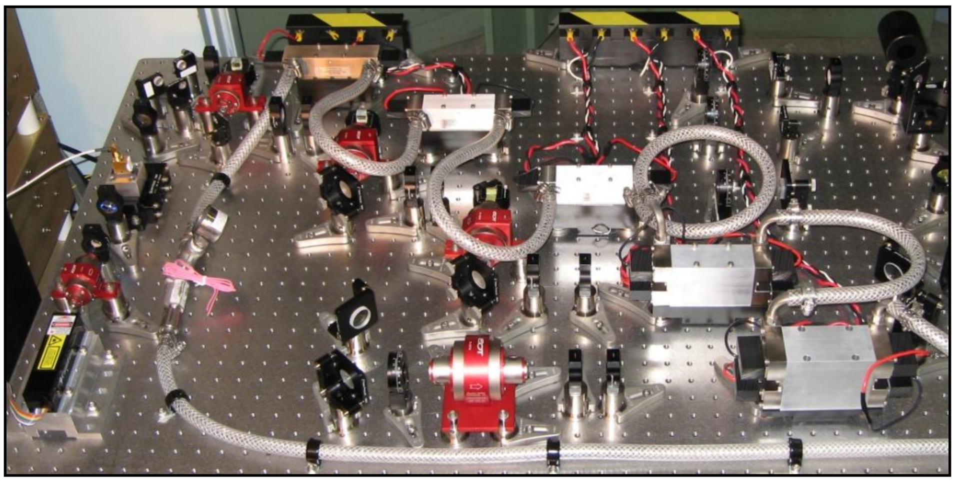

Figure 2. Photograph of upgraded pulse burst laser system with five laser amplifiers.

After amplification the high-energy pulses (>10 mJ/pulse) are frequency-doubled to 532 nm (green), a wavelength useful for fluid measurements, by use of an 8mm x 8 mm x 10 mm KTP Type II nonlinear crystal. A telescope is used to reduce the beam diameter from 12 mm at the exit of the amplifier chain to approximately 5 mm at the entrance face of the crystal to increase light intensity and more strongly drive the optical nonlinearity of the material. The crystal is angle-tuned at room temperature to achieve the phase matching condition. To generate light at 266 nm (ultraviolet), a similar harmonic conversion process is used, with two crystal materials being actively investigated. The first, Type I KDP, is commonly found in high-power Nd:YAG laser systems for generation of second, third, and fourth harmonics. The other material is Type I BBO, which possesses a much higher nonlinear coefficient than KDP, but has a much lower angular acceptance bandwidth, requiring excellent beam quality and collimation to achieve high efficiencies.[17] Figure 3 provides a photo and outline of the harmonic generator setup.

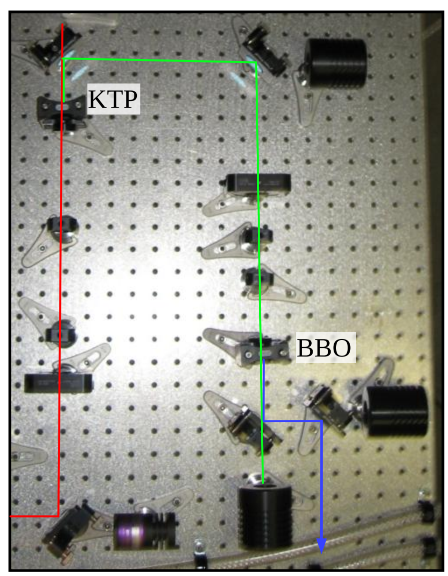

Figure 3. Photograph of harmonic generators for 532 nm and 266 nm light.

B. Results

The high configurability of the upgraded flashlamp controllers permits significant optimization over a wide range of operating conditions from kHz to MHz rates and at various pulse energies. Two particular system configurations were selected and optimized, first for generation of high individual pulse energy to demonstrate high-speed acetone PLIF, and also for high pulse repetition rate to demonstrate high-speed 3-D flow visualization.

To achieve a fluorescence signal level distinguishable from the noise floor of available cameras, significant pulse energies at 266 nm (> 1 mJ/pulse) are needed. By reducing the pulse repetition rate, and thus increasing the time between laser pulses (4 µsec at 250 kHz), substantial "gain refilling" can occur in the laser amplifiers between pulses. As the pulse repetition rate is further reduced, additional gains in individual pulse energy can be achieved, limited only by the onset of parasitic lasing between pulses and the length of the flashlamp pump pulse. Repetition rates lower than 250 kHz were not chosen in this study to prevent damage to optical components, particularly the nonlinear optical crystals. However, single pulses utilized during system alignment reached powers exceeding 200 mJ/pulse. Planned upgrades to be discussed later will ease this restriction.

To record pulse energies, a thermopile power sensor is used which acts as an energy integrator. By dividing the reported power by the overall system repetition rate and the number of pulses in each burst, an approximate per-pulse energy is obtained. For 68-pulse bursts at 250 kHz operation, the fundamental output at 1064 nm is approximately 72 mJ/pulse. The conversion to 532 nm yields a pulse energy of 20 mJ/pulse, indicating a harmonic conversion efficiency of 28%. The beam quality at this point was high enough to utilize the BBO crystal for conversion to 266 nm. The final output energy at 266 nm is 1.7 mJ/pulse, a conversion efficiency of 8.5%.

To reduce skew during a 3-D image acquisition, the laser is operated at the maximum speed of the camera, 500 kHz. The pulse separation time of 2 µsec is half that of the 250 kHz configuration. Accordingly, the pulse energies are approximately halved. The fundamental output is 30 mJ/pulse, and the conversion to 532 nm yields 7 mJ/pulse, an efficiency of 23%. This configuration was not used for high-speed PLIF; however, to provide comparison to the 250 kHz case, conversion to 266 nm was also tested. This resulted in a pulse energy of 0.3 mJ/pulse, far too low for practical fluorescence measurements.

A notable difference between the two configurations is the harmonic conversion efficiencies. As the incident energy decreases, the nonlinear drive in the crystal(s) also decreases, resulting in reduced harmonic output. For single test pulses of over 200 mJ/pulse, harmonic conversion efficiencies of 50% and 12.5% to 532 nm and 266 nm, respectively, were achieved.

III. Flow Facility and Experimental Arrangement

Two lab-scale flow facilities were used in this study, a small-scale high speed jet to demonstrate 2-D acetone PLIF, and a larger axisymmetric round jet used for the development of 3-D image processing techniques.

A. Small-Scale High-Speed Jet

A 3 mm diameter round jet was used for acetone PLIF for ease of uniform acetone seeding. A high-pressure regulated nitrogen bottle is connected to a pressure vessel containing acetone fluid. By introducing the nitrogen at the bottom of the tank, it bubbles up through the acetone and a portion of the acetone becomes a vapor. This high-pressure acetone-seeded flow is connected to a servo valve for easy operation, and a barbed connector, typically used for connecting vinyl tubing. This small diameter, straight connector serves as the high speed jet nozzle. For all experiments herein, the nozzle back pressure was approximately 40 psi, enough to drive the jet at a high subsonic velocity.

B. Axisymmetric Round Jet

To properly showcase the advantages of 3-D flow visualization, a low-speed round jet is used. This flow field possesses a combination of strong axisymmetric features such as ring vortices and demonstrates more complex 3-D features such as the transition to turbulent flow in the far-field. A more detailed study of the 3-D flow physics is currently under investigation and can be found in Ref. 10. The jet facility consists of a converging nozzle attached to a settling chamber with honeycomb and a perforated plate used at the nozzle inlet for flow conditioning. The settling chamber and nozzle are placed in an aluminum cage enclosure that is covered with black felt to mitigate room drafts and to reduce reflections. This enclosure also allows dot cards and other calibration tools to be easily placed at any location around the jet. Seed particles are generated in a secondary chamber using an ultrasonic mister to create small water droplets that are mixed with the airflow delivered to the nozzle. The nozzle has a contraction length of 165 mm and an exit diameter of 30.5 mm. The jet velocity at the exit was measured using a pitot probe to be approximately 3.3 m/s, corresponding to a Reynolds number based on jet diameter of approximately 6700. An example picture was taken using a traditional handheld digital camera with a long exposure time, as shown in Figure 4. This image clearly shows the rapid breakdown of laminar flow and the creation of rich 3-D flow features.

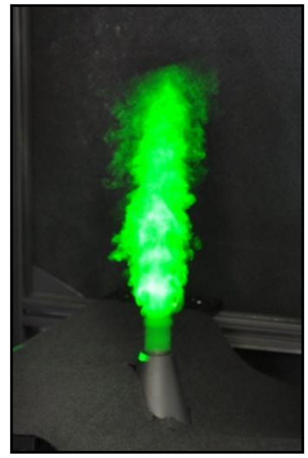

Figure 4. Picture of Round Jet taken during laser scan.

IV. Image Processing Development

The quality of the individual images and the entire image sequence is a function of the laser sheet intensity, camera depth of field, camera field of view, and the method of operation of the camera. The characterization of these effects and the development of proper correction procedures is necessary to yield high-quality 3-D data. The Ultra68 combines several high-speed imaging methods in order to achieve framing rates as high as 500,000 fps over 68 frames. First, light entering the camera is divided using a four-way beamsplitter, creating four separate optical paths. Identical images are thus formed on the surface of a four-quadrant image intensifier. Each quadrant of the intensifier is controlled independently allowing for high frame rates to be achieved by firing each quadrant in succession. A 2k x 2k CCD sensor is located behind the intensifier to record the images formed in the four quadrants. Additionally, the CCD is “masked,” where 16 out of 17 pixels are covered and used for high-speed charge storage, while a single pixel is sensitive to light.

This arrangement has several consequences for reconstruction of 3-D images. First, the intensifier, while making the system extremely sensitive, adds a significant amount of noise to the images. Second, the images formed on each of the quadrants must be recombined to a common image plane with sub-pixel accuracy. Furthermore, the characteristics of each image (i.e., gain uniformity, dark field, optical distortion, etc.) are dependent on the quadrant the image corresponds to. Likewise, all corrections performed take into account the dependency of image distortions on quadrant.

The initial development of many corrections for these effects has previously been reported by Lynch and Thurow,[18] and has been extensively improved. A brief description of the individual corrections is given here, followed by a more in-depth explanation of an image “ghosting” phenomena and a correction method that has been developed and implemented. Additionally, a novel method for correcting for laser sheet intensity and pulse-to-pulse intensity variations is described.

A. Flat Field and Spatial Corrections

The first correction performed is a flat-field correction, which corrects for slight differences in sensitivity of individual pixels on the CCD. These differences can be caused by non-uniform materials in the CCD or slight misalignments in the individual optical paths within the camera. Using a 60-watt frosted light bulb illuminating a sheet of paper and defocusing the lens, a uniform-intensity field is presented to the CCD. Software provided by the camera manufacturer takes multiple images and creates a set of individual pixel correction coefficients that when applied to each image, result in a uniform field. This set of coefficients is stored and used by the camera to correct all subsequent images. Additionally, to correct for any possible surrounding sources of light, such as specular reflections, a dark image is subtracted from all image data.

To create accurate 3-D reconstructions, the image data must be accurately calibrated to the 3-D physical space of the measurement volume. As the laser sheet scans through the measurement volume, there is a corresponding change in camera field of view, resulting in a 3-D trapezoidal measurement volume, illustrated in Figure 5. Additionally, due to the multiple optical paths within the camera, a slight 1-2 pixel “jitter” occurs from frame to frame. These distortions are simultaneously corrected using a dot-card alignment process. To provide maximum dot contrast compared to a printed sheet of dots, a back-illuminated dot card was constructed from an aluminum plate by drilling holes in a precise grid pattern, with a dot spacing of 0.5 in, and dot diameter of 0.125 in. This card was mounted on a translation stage and positioned at the rear image plane and the front image plane. The dot locations for each plane were found using a center-of-mass dot-finding technique, and the dot locations at the intermediate image planes were found using linear interpolation. Once the dot locations are determined, all of the images in a sequence can be mapped to a common grid. MATLAB is used to define the common grid and implement image transformations through the `create_tforms` and `imtransform` functions.

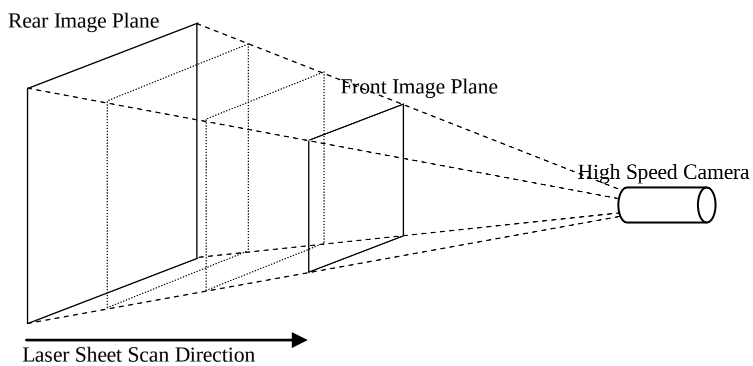

Figure 5. Field of View Change within Measurement Volume.

B. Pulse and Laser Sheet Intensity Variation Correction

The approximately Gaussian laser beam produced by the pulse burst laser system, when passed through a cylindrical lens, becomes a laser sheet with a similar intensity profile. This intensity distribution accentuates flow features near the center of the sheet, effectively reducing the usable region of the data set. Previous work has employed an in-situ calibration method where seeding characteristics of the flow field being studied are utilized to form average laser profiles and corrections. This approach is not suitable for achieving correction of instantaneous laser sheet profiles, which can fluctuate drastically from a mean profile due to thermal effects inherent in the high-power, high-gain nature of the laser system. Additionally, while the laser system is designed to produce relatively uniform bursts of pulses, there is a measurable difference in energy (on the order of 10%) between each pulse. A correction method has therefore been designed to simultaneously correct for both of these distortions.

After passing through the flow, the laser sheet exits the test cage and is projected onto a flat surface at an approximately 45 degree incidence angle. Each laser sheet appears as a distinct line separated by a distance due to the laser sheet scanning. A Cooke Corporation Sensicam QE camera is placed normal to the surface to image the lines. The Sensicam QE is a peltier-cooled, high-sensitivity CCD camera with a maximum resolution of 1376 x 1040 pixels. This high resolution allows for very accurate determination of both sheet intensity profile and pulse energy variation. An example image produced using this setup is shown in Figure 6.

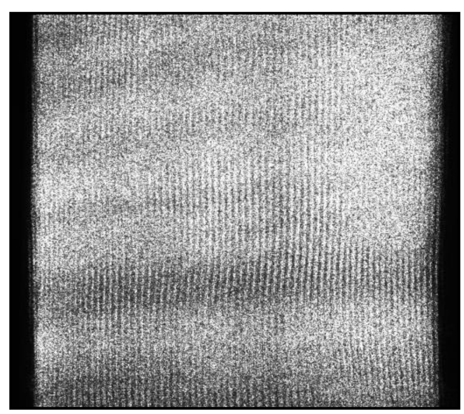

Figure 6. Pulse and Laser Sheet Intensity Correction Image.

Each image acquired using the Sensicam is processed using a custom MATLAB program, which identifies the location of each of the lines, determines a line intensity profile, and measures the relative intensity contained in each pulse. These profiles are shown in Figure 7. Simple geometry is used to scale the line intensity profile measured at the flat plane to the measurement volume.

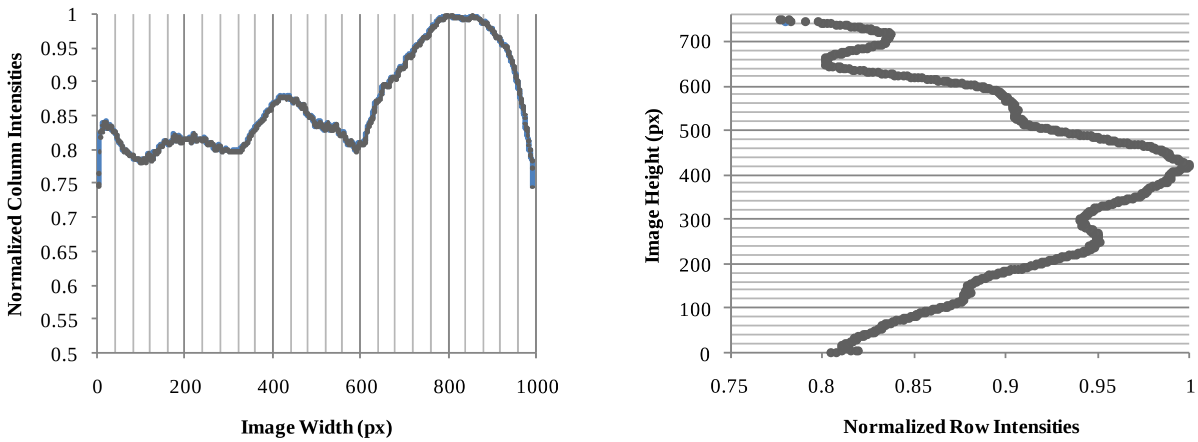

Figure 7. Pulse-to-Pulse Energy Variations (left) and Laser Sheet Intensity Profile (right). *The intensity axes are exaggerated for emphasis, and represent laser pulse energy and sheet intensity variations* ***of < 20%.***

C. Ghost Image Correction

Ghosting is an image artifact associated with the architecture of the Ultra68 camera where a low-intensity imprint of an image taken in one frame is evident in another frame. The exact cause of the artifact is unknown, but is believed to be due to the fluorescence decay time of the phosphor screen within the intensifier or charge remaining on the CCD during image storage and readout.

To quantify and correct for ghosting, a correction method has been developed which treats the image in frame m of the image sequence, I_m, as a linear combination of the signals, S, that comprise the image sequence, as shown in Eqn. 1. In this equation, n is the total number of frames in each sequence, equal to 68 for the Ultra68 camera, and a_i is a correction coefficient that must be determined.

$$I_m = \sum_{i=1}^{n} a_i S_i \tag{1}$$

This equation can be written in matrix form to describe an entire image sequence and can be inverted to solve for the individual signals, as shown in Eqn. 3.

$$\boldsymbol{I} = \boldsymbol{AS} \tag{2}$$

$$\boldsymbol{S} = \boldsymbol{A}^{-1}\boldsymbol{I} \tag{3}$$

The $\boldsymbol{A}$ coefficient matrix is determined by high-speed imaging of a laser sheet scanning across a flat sheet of dark paper. By timing the camera to coincide with the laser pulses, the laser sheet appears as a thin line that moves through the image sequence as shown by the cropped frames in Figure 8. Artifacts are clearly visible in these images, and provide a means for determining the off-diagonal elements of the coefficient matrix.

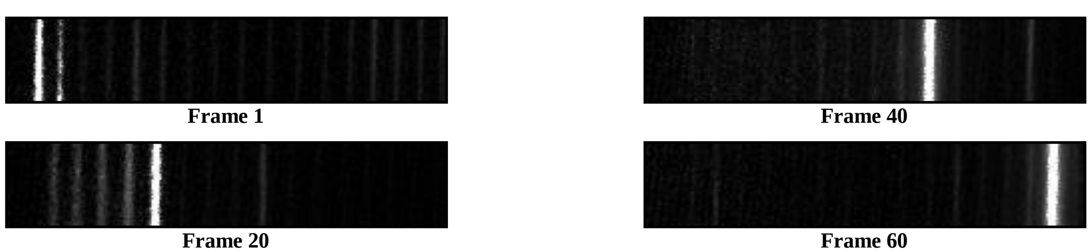

Figure 8. Scanning Method for Ghost Correction.

A MATLAB program has been developed which finds the location of the laser sheet in each frame. Using these coordinates, the program goes through each frame and determines the residual intensity of laser energy from each of the pulses that appears as an artifact in the image. In all cases, the columns of each image frame are summed, to reduce the influence of noise on intensity determination. Thus, each row of $\boldsymbol{A}$ contains the intensity of the main pulse, and the intensity of the artifacts in the remaining columns. By multiplying the original image data by $\boldsymbol{A}^{-1}$, the effect of ghosting becomes negligible and additional contrast in the images can clearly be seen, as shown in Figure 9.

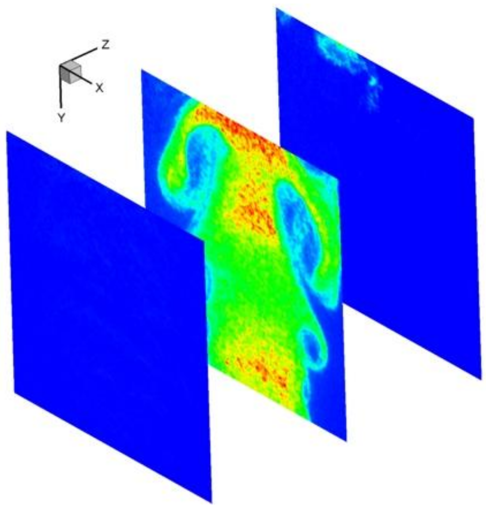

Figure 9. Slices 1, 34, and 68 of a image sequence, with ghosting correction (left), and without ghosting correction (right).

An assumption is made with this correction method that the ghosting phenomenon is uniform throughout each image (i.e., the upper region of an image does not deposit stronger artifacts than the lower region). The technique is currently being validated and expanded using a single pulse to illuminate an entire frame and deposit artifacts on the remaining frames of the sequence, rather than using a scanned sheet. By acquiring 68 sequences with the pulse delayed to occur at different frames, a similar analysis can be performed.

V. Results

The first results presented are of 250 kHz acetone PLIF. Figure 11 presents four images (out of a possible 68) of acetone PLIF conducted on the small-scale high speed jet. These images use flat field, dark image, and ghosting corrections. To generate a large enough usable signal, the Ultra68 intensifier was set to the highest gain setting, and the f/# of the lens was placed at the fully open setting f/2.8. However, signal levels were still small, and prevented us from utilizing the full dynamic range of the Ultra68. The small beam diameter exiting the fourth-harmonic generator also limited the minimum thickness of the laser sheet, contributing to slightly smaller signal levels, and blurred images. The jet can clearly be seen in every image, and the spatial growth downstream of the nozzle is noticeable. These images confirm that 3-D acetone LIF is possible using pulse burst laser sources, and can be readily adapted for 3-D measurements.

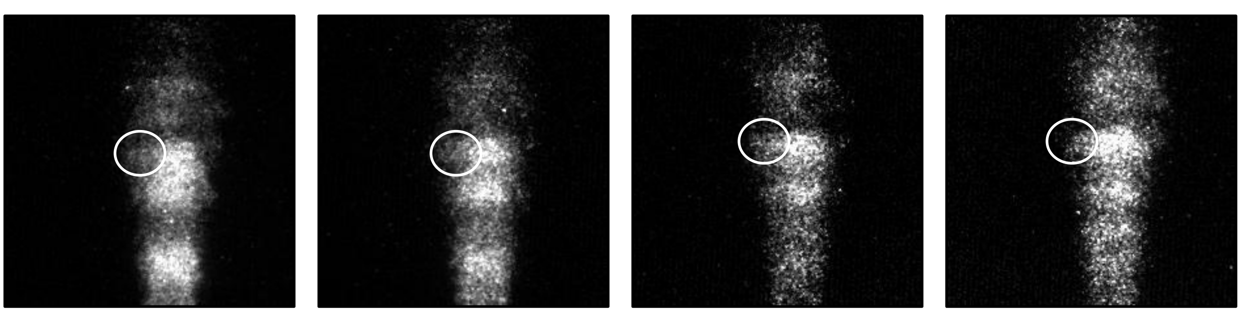

Frame 1	**Frame 2**	**Frame 3**	**Frame 4**
t = 0 μsec	**t = 4 μsec**	**t = 8 μsec**	**t = 12 μsec**

Figure 10: Four (out of a possible 68) frames of Acetone PLIF at 250 kHz. *The circle highlights a possible eddy structure that its shedding off of the jet core.*

Figures 11 through 13 showcase the application of 3-D reconstruction techniques and corrections to Mie scattering flow visualization performed on the axisymmetric round jet. Tecplot, a commercial software package designed for use with CFD and numerical data, is used to display the 3-D image. Figure 11 presents slices along the jet centerline axis with a translucent isosurface that delineates the boundary between the seeded particles in the jet and ambient fluid. The y-axis in this image has been stretched in order to completely show the individual slices. Note, the scanning direction was across the jet, while this representation shows data planes along another dimension. This is a distinct advantage of 3-D volumetric data, where slices along any direction can be used to better elucidate flow features that are prominent in particular dimensions. For the round jet flow field, Figure 11 provides a unique insight into the breakdown of centerline axis symmetry at the onset of transition.

Figure 12 explores the concept of iso-surfaces to define two arbitrary boundaries of intensity to mark the jet potential core and the surrounding fluid. This surrounding fluid becomes entrained in the shear layer instability resulting in mixing of ambient and jet fluid and a reduction in seeding particle number density and thus intensity values. In this image, the core is clearly defined with very little large or small scale disturbance. However, the addition of the translucent fluid at a lower intensity level shows clear evidence of a large vortex ring encircling the jet.

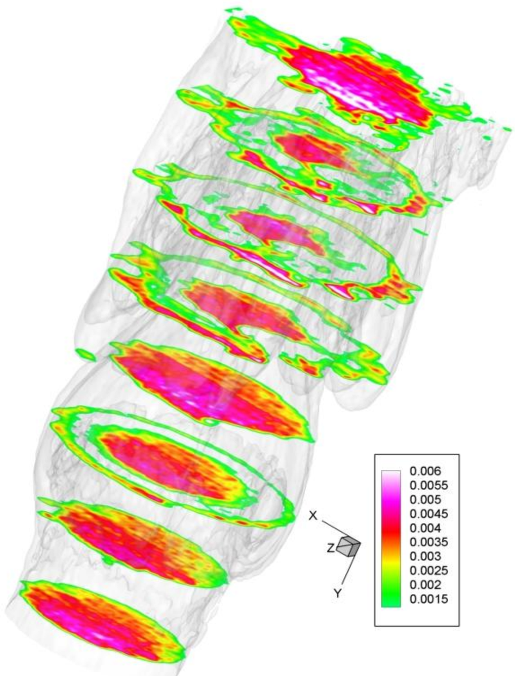

Figure 11. **Exploded view along the jet centerline axis.**

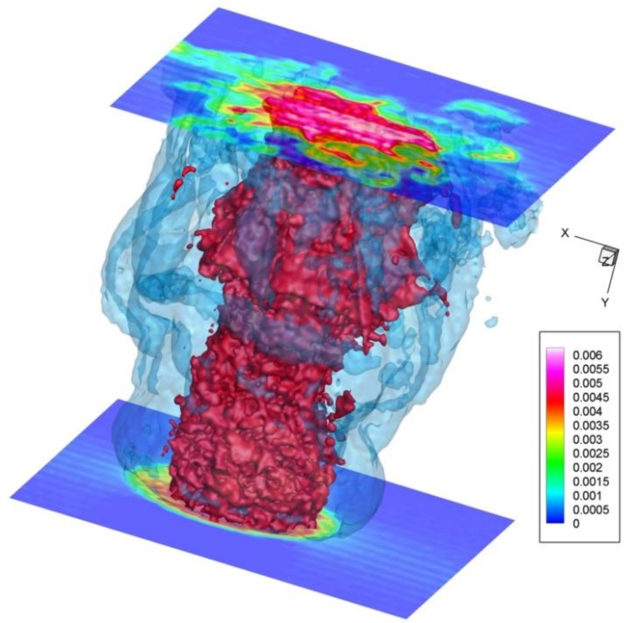

Figure 12: Isosurface visualization with opaque "core" fluid and translucent surrounding fluid

Figure 13 revisits the slicing concept to show how the Ultra68 camera actually acquires the images, e.g., these planes are the 2-D images captured by the camera. This image shows the particular effectiveness of the laser sheet intensity normalization and ghosting corrections, as almost no distortion due to those two phenomena is noticeable.

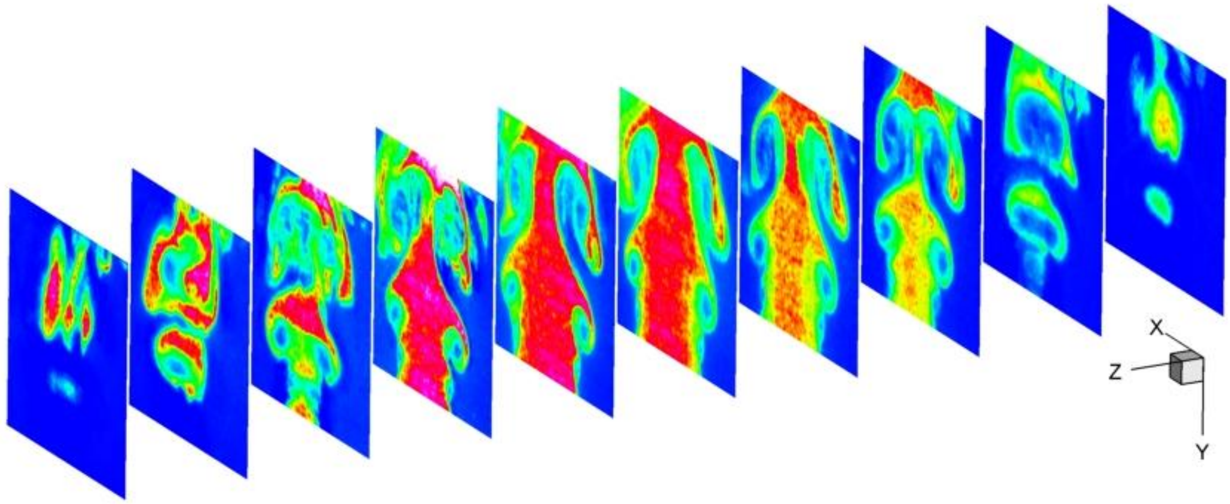

Figure 13. Image Slices taken along the scanwise direction. *This represents the images taken by the camera as the laser sheet sweeps through the flow field.*

VI. Conclusions and Future Work

The preliminary steps for the development of 3-D acetone LIF have been demonstrated, including upgrades to the pulse burst laser and investigation of 3-D reconstruction and calibration methods. 2-D acetone PLIF was achieved at 250 kHz, a repetition rate high enough to be useful for laser sheet scanning methods. The low signal levels indicate the need for increased laser pulse energy. Accordingly, work is underway on the pulse burst laser to increase both fundamental beam quality and laser energy using a stimulated brioullin scattering (SBS) mirror, commonly used in high-power laser amplifiers and a component in other pulse burst laser systems. The mirror is a nonlinear optical cell, which exhibits high reflectivity only with high input energies. This acts as a low-intensity filter to prevent gain drainage from occurring in the system. Additionally, it acts as a wavefront phase-conjugator, which when used in a double-pass amplifier configuration, increases the beam quality by nullifying the distortions caused by thermal loading of amplifier rods.

Image processing techniques for 3-D data sets have been extensively developed for particle scattering flow visualization data. Corrections in laser intensity, camera sensitivity, and spatial calibration have been considered and investigated. The procedures developed can be directly applied to 3-D LIF to provide accurate volumetric measurements of concentration, density, and other flow properties. The instantaneous three-dimensional measurement of these properties is unique to 3-D LIF and is not possible with any other laser diagnostic technique.

Acknowledgments

The support of the U.S. Army Research Laboratory and the U.S. Army Research Office is gratefully acknowledged. The author would like to thank Dr. Brian Thurow for his invaluable assistance, advice, and time given in this particular work, and throughout the author's undergraduate career. Additionally, the author thanks Chase Foster with assistance in constructing the acetone seeding system, and David Wall for assistance in designing mounts and equipment for the upgraded pulse burst laser system.

References

[1] Lozano, A., Yip, B., and Hanson, R.K., "Acetone: a tracer for concentration measurements in gaseous flows by planar laser induced fluorescence," *Experiments in Fluids*, Vol. 13, pp. 369-376, 1992.

[2] Papamoschou, D., and Bunyajitradulya, A., "Evolution of large eddies in compressible shear layers," *Physics of Fluids*, Vol. 9, pp. 756-765, 1997.

[3] Catrakis, H.J, Garcia, P.J. and Nathman, J.C., “Cumulative Aero-Optical Interactions Along Laser Beam Propagation Paths: Experiments and Computations,” AIAA Paper 2006-1495, 2006.

[4] Kychakoff, G., Paul, P.H., Van Cruyningen, I., and Hanson, R.K., “Movies and 3-D Images of flowfields using planar laser induced fluorescence,” *Applied Optics*, Vol. 26, pp. 2498-2500, 1987.

[5] Yip, B., Schmitt, R.L., and Long, M.B., “Instantaneous three-dimensional concentration measurements in turbulent jets and flames,” *Optics Letters*, Vol. 13, pp. 96-98, 1988.

[6] Patrie, B.J., Seitzman, J.M., and Hanson, R.K., “Instantaneous Three-Dimensional Flow Visualization by Rapid Acquisition of Multiple Planar Flow Images,” *Optical Engineering*, Vol. 33, pp. 975-980, 1994.

[7] Island, T.C., Patrie, B.J., Mungal, M.G., and Hanson, R.K., “Instantaneous Three-Dimensional Flow Visualization of a Supersonic Mixing Layer,” *Experiments in Fluids*, Vol. 20, pp. 249-256, 1996.

[8] Hult, J., Omrane, A., Nygren, J., Kaminski, C.F., Axelsson, B., Collin, R., Bengtsson, P.-E., and Alden, M., “Quantitative Three-Dimensional Imaging of Soot Volume Fraction in Turbulent Non-Premixed Flames,” *Experiments in Fluids*, Vol. 33, pp. 265-269, 2002.

[9] Thurow, B., Lynch, K., “Development of a High-Speed Three Dimensional Flow Visualization Technique,” accepted for publication in *AIAA Journal*, January 2009.

[10] Thurow, B. and Lynch, K., “3-D POD Analysis of a Naturally Excited Jet,” AIAA Paper 2008-4067, June 2008.

[11] Wu, P., Lempert W., Miles, R., “Megahertz Pulse-Burst Laser and Visualization of Shock-Wave/Boundary-Layer Interaction,” *AIAA Journal*, Vol. 38, pp. 672-679, 2000.

[12] B. Thurow, N. Jiang, M.Samimy, and W. Lempert, “Narrow-Linewidth Megahertz-Rate Pulse-Burst Laser for High-Speed Flow Diagnostics,” *Applied Optics*, Vol. 43, pp. 5064-5073, 2004.

[13] M. Wernet and A. Opalski, “Development and application of a MHz-frame rate PIV system,” AIAA Paper 2004-2184 (2004).

[14] A. Kastengren, J.C. Dutton and G. Elliott, “Time-Correlated Visualizations of Supersonic Blunt-Base Cylinder Wakes,” AIAA Paper 2005-1346 (2005).

[15] Thurow, B., Satija, A., and Lynch, K., “3rd generation MHz rate pulse burst laser system,” accepted for publication in *Applied Optics*, September 2008.

[16] Jiang, N., Webster, M.C., and Lempert, W.R., “Advances in generation of high-repetition-rate burst mode laser output,” *Applied Optics*, Vol. 48, pp. B23-B31, 2009.

[17] Koechner, W., *Solid-State Laser Engineering*, 6th ed., Springer, New York, 1999, Chap. 10.

[18] Lynch, K., Thurow, B., “Investigation of Image Processing Steps for Reconstruction of Three-Dimensional Flow Visualization Images,” AIAA Paper 2008-4269, June 2008.